e-ISSN: 2689-4934

Available online at
http://uppp.uitm.edu.my/online-issues.html

ESTEEM Academic Journal Vol 22, September 2025, 150-166

ESTEEM
Academic Journal
(EAJ)

# Comparative kinetic analysis of $TiO_2$ and Zeolite ZSM-5 catalysts in the *in situ* epoxidation of palm kernel oil

Nur Amira Dewi Zulkifli Selvakummar[1], Siti Khatijah Jamaludin[2*], Siti Aminah Md Ali[2]

[1]*Faculty of Chemical Engineering, Universiti Teknologi MARA, 40450, Shah Alam, Selangor, Malaysia.*
[2]*Faculty of Chemical Engineering, Universiti Teknologi MARA Cawangan Pulau Pinang, 13500 Permatang Pauh, Pulau Pinang, Malaysia.*

ARTICLE INFO

*Article history:*
Received 26 May 2025
Revised 1 August 2025
Accepted 20 August 2025
Online first
Published 20 September 2025

*Keywords:*
Palm Kernel Oil
*In situ* Epoxidation
$TiO_2$ Catalyst
Zeolite ZSM-5 Catalyst
Kinetic Study
Langmuir-Hinshelwood Mechanism

*DOI:*
10.24191/esteem.v21iSeptember.7132.g5031

ABSTRACT

*In situ* epoxidation is a well-established technique for chemically modifying plant-based oils to produce epoxide compounds, which serve as important intermediates in the synthesis of various industrial chemicals. However, homogeneous catalysts in epoxidation face major drawbacks such as high waste generation, difficult separation, non-recyclability, and high costs. Therefore, heterogeneous solid catalysts are needed to overcome these issues and enable a more sustainable process. This research investigates the catalytic efficiency of $TiO_2$ and zeolite ZSM-5 in the *in situ* epoxidation of palm kernel oil (PKO) under different operating conditions. The reaction was conducted in a semi-batch, one-pot system using formic acid as the oxygen donor and hydrogen peroxide as the oxidant, with trials at 45 °C, 55 °C, and 65 °C. Reaction time was not fixed but determined by the point at which a decrease in experimental oxirane oxygen content ($[OOC]_{exp}$) was first detected. Both catalysts were tested at a loading of 5 g to evaluate their effectiveness in enhancing oxirane content (RCO%). Zeolite ZSM-5 showed superior performance, achieving 46% double-bond conversion to epoxide and stabilising epoxide rings within just two minutes at 55 °C. Kinetic analysis using the Langmuir–Hinshelwood model confirmed that the process was not influenced by external mass transfer resistance at an agitation speed of 850 rpm. The surface reaction, particularly performic acid formation, was identified as the rate-determining step. At 55 °C, the surface reaction rate constant was 14.68 L/g catalyst, and the activation energy across the tested temperature range was 147.23 kJ/mol. Overall, ZSM-5 proved to be an effective catalyst for the green epoxidation of PKO, with kinetics well described by the Langmuir–Hinshelwood mechanism.

[2*] Corresponding author. *E-mail address*: sitikhatijah@uitm.edu.my

https://doi.org/10.24191/esteem.v21iSeptember.7132.g5031

## 1. INTRODUCTION

Versatile products can be produced from plant oil and animal fat due to their characteristics as renewable sources. These renewable sources are environmentally friendly and biodegradable. Plant-derived oils can be functionally modified through both chemical methods, such as interesterification and hydrogenation, as well as enzymatic processes that offer improved selectivity and sustainability [1-2]. Various plant-based oils exist, such as soybean oil, rapeseed oil, palm oil, and palm kernel oil (PKO). PKO is specifically extracted from the kernel, or endocarp, of the palm fruit. To produce crude palm oil, fresh palm fruits undergo sequential processes including sterilisation, stripping from the bunch, digestion, oil extraction, and clarification to ensure efficient oil recovery [3-4]. Crude PKO undergoes physical and chemical refining to produce RBD PKO (refined, bleached, and deodorized). Plant oils are preferred as raw materials because they contain higher levels of unsaturated fatty acids compared to animal fats, These unsaturated fatty acids are important in food processing applications because they contribute to lower cholesterol levels. Unsaturated fatty acids, due to their reactive double bonds, are highly prone to oxidation and play a significant role in driving oxidative reactions in oleochemical systems [5].

The rising demand for renewable-based consumer products has led to the expansion of crop cultivation areas and advancements in analytical technologies to support efficient processing and quality assurance [6-7]. PKO is widely modified through processes such as blending, hydrogenation, fractionation, interesterification, and epoxidation to tailor its physical and chemical properties for oleochemical applications [8-9]. Among all chemical modifications, the epoxidation process is favoured in the oleochemical industry for its ability to produce specialty products.

Epoxidation is a chemical process in which an oxygen atom is introduced across the carbon–carbon double bond of unsaturated fatty acids, transforming olefins into epoxide compounds that act as key intermediates in subsequent chemical reactions [10]. Traditional epoxidation methods, such as non-catalytic chlorine-based processes, co-epoxidation, and preformed epoxidation, have been reported in the literature. These methods, however, suffer from significant drawbacks. Chlorine-based processes produce chlorinated byproducts and cause corrosion issues [11], while co-epoxidation shows poor selectivity and generates waste [12]. Moreover, preformed epoxidation can result in hazardous spikes in peracid concentration, leading to instability or even explosive conditions [13]. To address these limitations, researchers developed the *in situ* epoxidation method, where peracid is generated directly from hydrogen peroxide ($H_2O_2$) and a carboxylic acid within the mixture, enabling safer operation, better control, and greater process stability [14]. Fig. 1 illustrates the reaction pathway involved in the *in situ* epoxidation process, where peracid formation and epoxidation occur sequentially and continuously within a single reaction system [15].

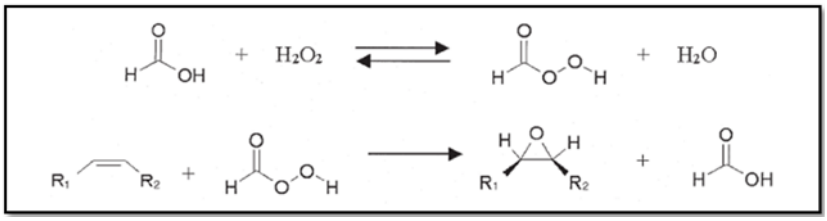


Fig. 1. *In situ* epoxidation process

Source: Mohd Zin *et al.*, 2020 [15]

The epoxy ring, also termed oxirane, plays a significant role in the manufacture of plasticising compounds and stabilisers for polymer-based materials due to its high chemical reactivity. Industries seek epoxidised oils with high oxirane content for use in lubricants, plasticisers, wood coatings, cosmetic

https://doi.org/10.24191/esteem.v21iSeptember.7132.g5031

formulations, pharmaceuticals, and as reactive additives in biofuels [16]. Epoxides are increasingly favoured in industry nowadays due to their unique properties, such as being highly strained and reactive. As an example in plastic industries, the higher amount of epoxy produced, the higher crosslinking of the cyclic formed, and produces high-quality plastics [17]. Epoxides are versatile intermediates that can undergo ring-opening reactions to form glycols, alcohol derivatives, hydroxyesters, and alkanolamines, enabling further functionalisation in chemical synthesis [10, 16]. Fig. 2. shows the ring-opening reactions of an epoxide.

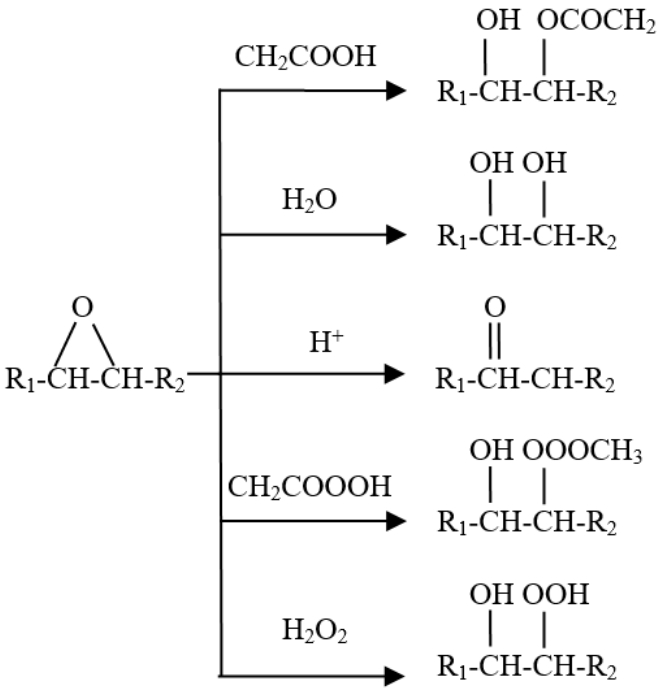


Fig. 2. Epoxide ring opening reactions

Source: Goud *et al.*, 2007 [19]

In current applications, *in situ* epoxidation typically relies on the use of catalysts to enhance both reaction speed and overall conversion. These catalysts are generally classified into two types: homogeneous and heterogeneous. Homogeneous acid catalysts, such as sulphuric acid ($H_2SO_4$), phosphoric acid ($H_3PO_4$), hydrochloric acid (HCl), and nitric acid ($HNO_3$), are commonly employed in *in situ* epoxidation systems. Despite their ability to accelerate the reaction, these catalysts are often associated with several drawbacks, including low selectivity, corrosion issues, the generation of salts, and the need for complex product purification processes [20]. To address these limitations, researchers have shifted toward developing heterogeneous catalysts, which offer improved operational advantages. Examples include vanadium-based oxides, mixed metal oxides such as $Al_2O_3$–$ZrO_2$, and sulfonated ion-exchange resins. These alternatives are known for better epoxide selectivity, simplified separation from reaction mixtures, and enhanced catalyst recyclability [21].

To evaluate the performance of different catalysts, this study explores the *in situ* epoxidation kinetics of PKO using heterogeneous catalytic systems. Conventional homogeneous catalysts, though effective, suffer from significant drawbacks such as high waste generation, difficulty in separation, non-recyclability, and high process costs. This limitation highlights the need to investigate heterogeneous solid catalysts as a

https://doi.org/10.24191/esteem.v21iSeptember.7132.g5031

more sustainable alternative. Specifically, titanium dioxide ($TiO_2$) and zeolite ZSM-5 were selected due to their proven catalytic activity, stability, and suitability in epoxidation reactions. Zeolite ZSM-5 is widely recognized for its high surface area, strong acidity, and shape selectivity, which enable efficient double-bond conversion and stabilisation of epoxide rings [10]. Meanwhile, $TiO_2$ offers photocatalytic properties, tunable surface hydroxyl groups, and high dispersion, which promote peroxo-species formation and enhance the interaction with hydrogen peroxide [22]. The effectiveness of these catalysts will be compared in terms of reaction rate, double-bond conversion to epoxide, and epoxide ring stability. The superior catalyst will then be employed for kinetic modelling using the Langmuir–Hinshelwood framework, a modelling approach that, to the best of our knowledge, has not been previously applied to this epoxidation system, thereby allowing determination of the rate constant and activation energy of the reaction.

## 2. METHODOLOGY

### 2.1 Materials

PKO was supplied by the Malaysian Palm Oil Board (MPOB). Formic acid (FA, 98% w/w, analytical reagent grade, R&M Marketing), hydrogen peroxide ($H_2O_2$, 30% w/w, R&M Marketing), glacial acetic acid (≥99.7%, analytical reagent grade, R&M Marketing), titanium dioxide ($TiO_2$, Degussa P-25, ≥99.5%), zeolite ZSM-5 (analytical grade, R&M Marketing), and anhydrous sodium sulfate ($Na_2SO_4$, ≥99%, analytical grade, R&M Marketing) were used as received. Hydrobromic acid (HBr, 47% w/w, R&M Marketing), crystal violet (indicator grade, R&M Marketing), and potassium hydrogen phthalate (≥99.5%, analytical grade, R&M Marketing) were also obtained from the same supplier for the standardization of 0.1 N HBr in acetic acid.

### 2.2 Pre-treatment of catalysts

The catalysts used in this study, mesoporous $TiO_2$ and zeolite ZSM-5, were subjected to calcination to improve their catalytic activity. Prior to use, both materials were placed in a furnace and heated at 500 °C for 5 hours in air, then allowed to cool naturally to room temperature inside the furnace before use. This thermal treatment removes organic residues, enhances surface acidity, and stabilises the pore structure, ensuring better performance during the *in situ* epoxidation process.

### 2.3 Experimental set-up

The *in situ* epoxidation process was conducted using a 500 mL beaker functioning as the reaction vessel, as illustrated in Fig. 3. A water bath was employed to maintain a consistent reaction temperature by minimizing heat loss around the beaker. To facilitate stirring, a motorised impeller was used. Temperature monitoring was performed by inserting a thermometer directly into the reaction mixture. The system included two burettes secured to a retort stand: one dispensed hydrogen peroxide dropwise, while the second was designated for sample titration using 0.1 N hydrobromic acid dissolved in acetic acid.

### 2.4 Experimental procedure

The *in situ* epoxidation began with the introduction of a measured quantity of PKO into the beaker reactor. Subsequently, formic acid and a catalyst (either $TiO_2$ or zeolite ZSM-5) were added to the system. A stirring speed of 450 rpm was selected to ensure effective mixing and avoid mass transfer limitations. Hydrogen peroxide was then introduced dropwise into the mixture, with the addition of the first drop marking the official start of the reaction time. Experiments were conducted at three set temperatures: 45 °C, 55 °C, and 65 °C. Samples were extracted at five-minute intervals for the determination of experimental oxirane oxygen conversion ($[OOC]_{exp}$) analysis and for evaluating the stability duration of the epoxide ring. To halt the reaction, anhydrous sodium sulfate was added to the sample vial, effectively quenching any further reaction. The sampling process was terminated once a decrease in $[OOC]_{exp}$ indicated the onset of

https://doi.org/10.24191/esteem.v21iSeptember.7132.g5031

epoxide degradation.

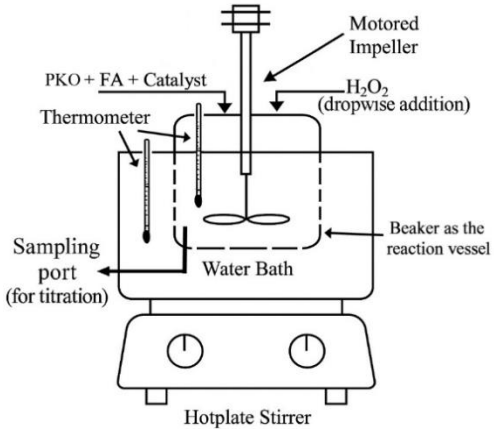


Fig. 3. Reactor set-up for *in situ* epoxidation of PKO

## 2.5 Analytical techniques

The method used was modified based on AOCS Tentative Method Cd 9-57 [23]. The $[OOC]_{exp}$ was determined by adding 8 g of hydrobromic acid (HBr) to 500 mL of glacial acetic acid. Then, approximately 0.4 g of the sample was dissolved in 10 mL of acetic acid. The titration was done by adding five drops of crystal violet indicator to the sample. The end point of this titration was when a bluish-green colour appeared for at least 30 seconds. The $[OOC]_{exp}$, expressed in moles per 100 g, was calculated using Eq. (1):

$$[OOC]_{exp} = \frac{\mathrm{T} \times N_{HBr} \times 1.6}{\mathrm{W}} \quad (1)$$

where T is the volume in mL of HBr solution required to titrate the sample, $N_{HBr}$ is the normality of the HBr solution and W is the weight of the sample in grams.

Based on this value, the relative conversion to oxirane (RCO%) was determined using Eq. (2):

$$(\mathrm{RCO\%}) = \frac{[OOC]_{exp}}{[OOC]_{theo}} \times 100\% \quad (2)$$

where $[OOC]_{theo}$, the theoretically obtainable maximum oxirane oxygen, was calculated based on Eq. (3):

$$[OOC]_{theo} = \left[\frac{\frac{IV_{PKO}}{2A_i}}{100 + \frac{IV_{PKO}}{2A_i} A_o}\right] x\ A_o\ x\ 100 \quad (3)$$

where $IV_{PKO}$ (iodine value of PKO) is 19, $A_i$ (molar mass of iodine) is 126.9, and $A_o$ (molar mass of oxygen) is 16. The basis for Eq. (3) is 100 g PKO sample.

https://doi.org/10.24191/esteem.v21iSeptember.7132.g5031

### 2.6 Kinetic study

The kinetics of the *in situ* epoxidation employing zeolite ZSM-5 as a solid catalyst were investigated using a mechanistic model based on Langmuir–Hinshelwood theory. To determine the relevant kinetic parameters, experimental data were analysed using non-linear curve fitting through the Levenberg–Marquardt optimisation technique implemented in Polymath. From this modelling process, both the rate constant and the energy barrier for the reaction were determined, with the activation energy obtained from the gradient of the Arrhenius plot.

## 3. RESULTS AND DISCUSSION

### 3.1 Epoxide solution appearance

The oxirane oxygen percentage (RCO%) was determined by measuring the remaining concentration of double bonds, following the procedure described in AOCS Tentative Method Cd 9-57. After the reaction, the solution displayed a pale-yellow colour. Upon the addition of a violet-coloured indicator, the mixture turned deep purple, as shown in Fig. 4. (a). Once titration was completed, the solution changed gradually to a bluish-green, as illustrated in Fig. 4. (b). The violet-to-bluish green colour change arises from protonation of the crystal violet indicator in the acidic medium. Initially, added HBr is consumed by reaction with double bonds, and the solution remains violet. Once all unsaturated sites are titrated, excess HBr protonates crystal violet, shifting its absorption spectrum to bluish green, which marks the titration endpoint [24]. This colour shift provided a visual confirmation of epoxide formation, with the intensity of the change corresponding to the extent of conversion of unsaturated bonds.

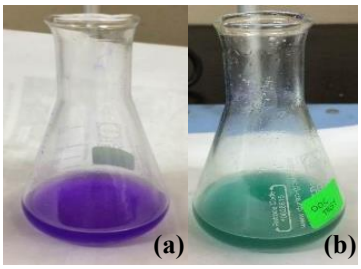


Fig. 4. Epoxide solution appearance

### 3.2 Optimum condition in *in situ* epoxidation of PKO

The primary outcome of the *in situ* epoxidation process is the generation of epoxidised PKO. In this work, the performance of the reaction was assessed based on two key factors: the relative oxirane yield (RCO%) and the stability of the epoxide ring. A higher RCO% reflects greater efficiency in converting unsaturated bonds into epoxide groups, indicating a more effective epoxidation process. Meanwhile, the duration of epoxide ring stability represents how long the three-membered ring structure can remain intact before undergoing ring-opening to form single bonds. Together, these parameters provide insight into both the conversion efficiency and durability of the formed epoxide.

*Optimum temperature*

The influence of reaction temperature (45 °C, 55 °C, and 65 °C) on the *in situ* epoxidation of PKO was evaluated using $TiO_2$ and zeolite ZSM-5 as catalysts, as illustrated in Fig. 5. For the ZSM-5-catalysed process, the highest oxirane content (RCO%) of 46.61% was obtained at 45 °C. In comparison, the values

https://doi.org/10.24191/esteem.v21iSeptember.7132.g5031

at 55 °C and 65 °C were slightly lower, measuring 45.56% and 38.99%, respectively. This indicates that 45 °C is the optimum temperature for maximum oxirane formation when using zeolite ZSM-5. Moreover, the epoxide rings formed at this temperature demonstrated enhanced stability, lasting approximately three minutes. At higher temperatures (55 °C and 65 °C), the maximum stability duration was consistently observed at two minutes.

A similar trend was observed for $TiO_2$, where the peak RCO% of 38.66% was achieved at 55 °C. At 65 °C, the RCO% slightly declined to 33.39%, while the lowest RCO% of 30.86% occurred at 45 °C. Notably, despite producing the lowest oxirane content, the epoxide rings formed at 45 °C exhibited a longer stability plateau, maintaining their structure for three minutes. Meanwhile, the maximum ring stability observed at 55 °C and 65 °C was again limited to two minutes, consistent with the ZSM-5 catalyst results.

Mohamed et al. [25] identified 55 °C as the optimum temperature for *in situ* epoxidation using $TiO_2$, which aligns with current findings. However, Goud et al. [19] proposed that lower temperatures could yield higher RCO%, particularly under pre-formed peracid conditions. In contrast, the present study employs an *in situ* generation approach where all reactants and catalysts are combined simultaneously. This integrated method results in different kinetic behaviour, particularly in epoxide ring formation and stability. As temperature increases, the rapid formation of performic acid tends to promote ring-opening reactions and reduce epoxide yield.

Despite showing strong epoxide stability at 45 °C, this condition leads to reduced RCO% in $TiO_2$-catalysed systems. For both catalysts, 65 °C consistently produced the lowest oxirane values, likely due to thermal degradation and increased side reactions. Therefore, within the moderate temperature range (45–60 °C), 55 °C offers a suitable compromise, balancing both epoxide stability and conversion efficiency. This supports the conclusion that 55 °C serves as the optimal temperature for *in situ* epoxidation of PKO under both $TiO_2$ and ZSM-5 catalysis, although 45 °C remains more favourable for ZSM-5 in terms of peak RCO%.

*Optimum catalyst*

Catalyst effectiveness in *in situ* epoxidation was evaluated based on surface area, with higher surface areas generally promoting improved reaction rates. Among the catalysts studied, zeolite ZSM-5 achieved a higher oxirane yield (RCO%) than $TiO_2$ at the same reaction temperature of 55 °C. In contrast, $TiO_2$ produced a lower RCO%, likely due to its limited porosity. This observation is consistent with earlier findings that mesoporous $TiO_2$ exhibits enhanced catalytic performance compared to its commercial counterpart, owing to greater pore volume and surface area [26]. Furthermore, incorporating transition metals such as iron into the $TiO_2$ structure can significantly enhance its activity [27]. These findings align with past studies involving the epoxidation of oils like methyl oleate and palm-based feedstocks.

Zeolite ZSM-5 acts as a robust solid-acid catalyst, valued for its structural and thermal stability in reactions such as olefin epoxidation. Its microporous framework offers a high density of Brønsted acid sites, creating favourable environments for epoxide formation. The superior catalytic performance of ZSM-5 has been attributed to its pore architecture and acid strength, which together enhance both activity and selectivity in oxidation reactions [28]. Hierarchical variants of ZSM-5, featuring added mesoporosity, further improve performance by facilitating better access for larger molecules and reducing diffusion limitations [29].

ZSM-5's unique framework and acidity make it an exceptionally active epoxidation catalyst. In particular, ZSM-5 is a microporous aluminosilicate zeolite with a crystalline pore network, high surface area, and a high density of strong Brønsted acid sites [10]. These features promote adsorption of the *in situ*-generated peracid and unsaturated fatty substrates, stabilising the transition state for the Prilezhaev reaction. For example, dendritic ZSM-5 (with enhanced external surface area) yielded much higher turnover frequencies in model epoxidations than conventional zeolite, demonstrating the benefit of its accessible acid sites [30]. By contrast, simple oxides like $TiO_2$ lack Brønsted acidity and shape-selective pores, which

https://doi.org/10.24191/esteem.v21iSeptember.7132.g5031

generally show lower activity in such peracid epoxidations.

In addition, catalyst pre-treatment via calcination plays a crucial role in improving catalytic efficiency. This thermal process removes organic residues and increases the surface area of acidic catalysts, making them more active than neutral counterparts. Calcination enhances both surface area and pore structure, leading to greater catalytic efficiency. In this study, calcined zeolite ZSM-5 demonstrated superior performance compared to $TiO_2$, confirming its suitability as an optimal solid acid catalyst for the *in situ* epoxidation of PKO.

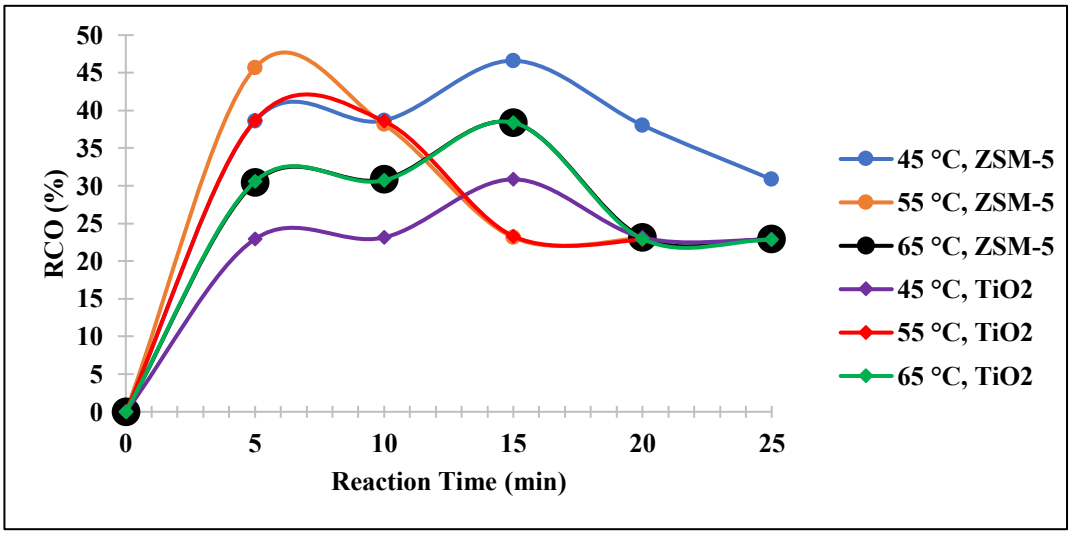


Fig. 5. Relative conversion to oxirane by using zeolite ZSM-5 and degussa P-25 $TiO_2$

### 3.3 Determination of mass transfer limitation through agitation speed

The influence of agitation speed on the *in situ* epoxidation rate using zeolite ZSM-5 at 55 °C was assessed, with results presented in Fig. 6. Experimental runs were conducted at various stirring speeds: 250 rpm, 450 rpm, 650 rpm, and 850 rpm. As illustrated in Fig. 6., the reaction rate increases markedly as the agitation speed rises from 250 rpm to 450 rpm, beyond which the change in RCO% becomes negligible. This plateau indicates that above 450 rpm, additional stirring provides minimal improvement in oxirane yield, particularly between 650 rpm and 850 rpm. It is widely recognised that agitation speeds above 500 rpm are typically sufficient to overcome external mass transfer resistance in a liquid-phase epoxidation system. Beyond this threshold, further increases in stirring speed do not significantly impact reaction kinetics. To eliminate limitations related to interfacial transport whether between solid–liquid phases or between two immiscible liquids, a sufficiently high agitation speed is required. Increased agitation reduces droplet size and enhances interfacial surface area, thereby improving phase contact and facilitating more efficient mass transfer across interfaces.

### 3.4 Kinetic study of heterogeneous catalytic *in situ* epoxidation of PKO

In this analysis, the kinetic model for the *in situ* epoxidation process focuses on reactions catalysed by zeolite ZSM-5 as a solid catalyst. The fundamental reaction pathway for *in situ* epoxidation of vegetable oils is outlined in Table 1, comprising Steps 1 to 5 [19]. The presence of a heterogeneous catalyst, however, introduces additional surface-mediated steps, including adsorption, surface interactions, and desorption which are characteristic of solid–liquid catalytic systems. These extended mechanisms are captured in

https://doi.org/10.24191/esteem.v21iSeptember.7132.g5031

Steps 6 through 10, reflecting the complete catalytic sequence in heterogeneous *in situ* epoxidation.

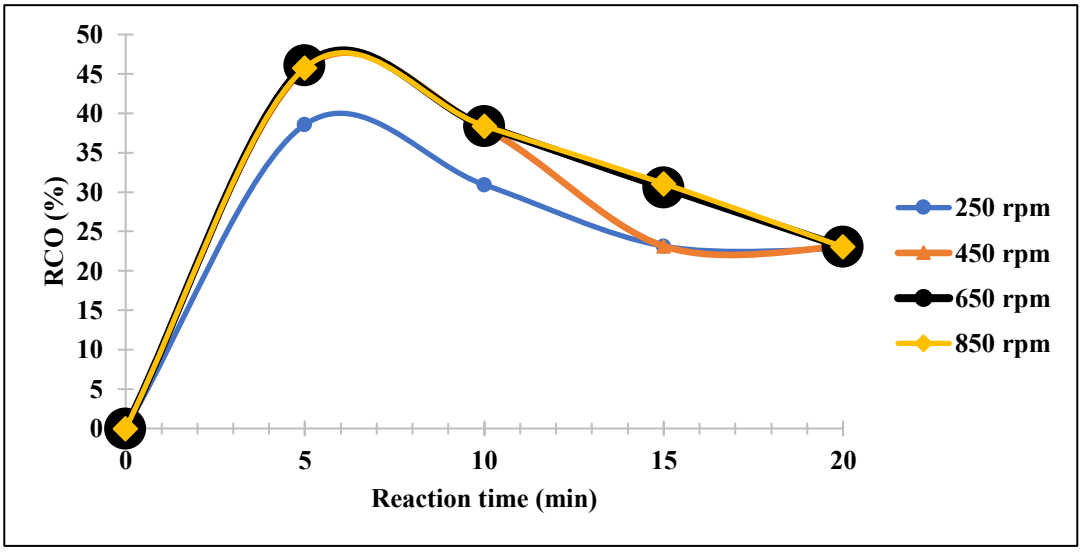


Fig. 6. Rates of *in situ* epoxidation of PKO catalysed by zeolite ZSM-5 under various speed

Table 1. Steps involved in the catalytic *in situ* epoxidation of vegetables oil

| Step | Descriptions | Mechanism |
|---|---|---|
| Step 1 | Performic acid is synthesised in the aqueous phase through the catalytic reaction between hydrogen peroxide and formic acid | *In situ* epoxidation of vegetables oils |
| Step 2 | The generated performic acid migrates from the aqueous medium into the oil phase | |
| Step 3 | Performic acid reacts with PKO, forming the epoxide and regenerating free formic acid | |
| Step 4 | The formed epoxide may degrade or undergo side reactions | |
| Step 5 | Released formic acid returns to the aqueous phase | |
| Step 6 | Reactants diffuse into the catalyst pore system | Additional heterogeneous catalytic steps in *in situ* epoxidation of vegetables oils |
| Step 7 | Adsorption of reactants onto the catalyst surface occurs | |
| Step 8 | Surface-level chemical interactions take place between catalyst and reactants | |
| Step 9 | Reaction products desorb from the catalyst surface | |
| Step 10 | Product molecules diffuse out of the catalyst pore structure | |

Zeolite ZSM-5 has been shown to facilitate performic acid formation without interfering with the subsequent epoxidation of PKO, while enhancing reaction kinetics and oxirane yield. Although pseudo-homogeneous kinetic models have been widely applied to describe *in situ* epoxidation, they are often inadequate for systems involving heterogeneous catalysts like zeolite ZSM-5, particularly at elevated temperatures. These models assume uniform reaction conditions and neglect surface phenomena, making them suitable only when catalyst–reactant interactions occur entirely in the bulk phase. In contrast, zeolite ZSM-5 possesses a well-defined microporous structure and high surface acidity, where catalytic activity is governed by surface adsorption, diffusion, and site-specific interactions. The Langmuir–Hinshelwood (L–H) model offers a more realistic framework for such systems by incorporating key surface-related steps: adsorption, surface reaction, and desorption. This mechanistic approach reflects the physical characteristics

https://doi.org/10.24191/esteem.v21iSeptember.7132.g5031

of solid acid catalysts and is particularly relevant at moderate temperatures, where surface coverage and competitive site adsorption can significantly influence reaction rates [31].

The *in situ* epoxidation of PKO using performic acid and zeolite ZSM-5 as a catalyst involves two key reaction steps. The first step is the acid-catalysed formation of performic acid from formic acid and hydrogen peroxide, as represented in Reaction (1):

$$HCOOH + H_2O_2 \rightleftharpoons HCOOOH + H_2O \text{ (acid-catalysed)} \quad (1)$$

The second step is the epoxidation of unsaturated compounds using performic acid as the oxidizing agent. This reaction is not catalysed and leads to the formation of epoxide rings, as illustrated in Reaction (2):

$$R_1–CH=CH–R_2 + HCOOOH \rightarrow R_1–CH(O)–CH(R_2) + HCOOH \quad (2)$$

To describe the reaction kinetics, the Langmuir–Hinshelwood (L–H) model was applied, which considers three elementary steps: adsorption of reactants, surface reaction, and desorption of products. Agitation at 850 rpm was sufficient to minimise mass transfer effects, as indicated by the unchanged RCO% beyond 450 rpm. Therefore, mass transfer limitations and pore diffusion are not addressed in this analysis.

For modelling purposes, the formation of performic acid was treated as the rate-determining step and incorporated into a heterogeneous catalytic framework. The L–H model was used to represent the catalytic behaviour, with the reaction kinetics expressed in the form of a differential equation. Parameter estimation was conducted using non-linear regression, specifically the Levenberg–Marquardt method, to fit experimental data to the proposed model.

The reaction kinetics were modelled under pseudo-batch reactor conditions using a differential rate law, where the rate of consumption of hydrogen peroxide (the limiting reactant) is described by Equation 3:

$$r_a = \frac{-dC_a}{dt} \quad (3)$$

In this kinetic model, Reaction 1 (performic acid formation) is treated as a heterogeneous catalytic reaction, whereas Reaction 2 (epoxidation step) is considered pseudo-homogeneous. The Langmuir–Hinshelwood (L-H) framework was used to describe the surface reaction behaviour for Reaction 1, and further model development is detailed in Table 2 for reactions labelled as Reaction 3 to Reaction 5.

Table 2. L-H approaches in heterogeneous catalytic of performic acid formation

| Reaction | Mechanism |
|---|---|
| Reaction 3: Adsorption | $k_a$<br>$FA + S \leftrightarrow FA•S$<br>$k_{-a}$ |
| Reaction 4: Surface Reaction | $FA•S + H_2O_2 \rightarrow PFA•S + H_2O$ |
| Reaction 5: Desorption | $k_d$<br>$PFA•S \leftrightarrow PFA + S$<br>$k_{-d}$ |

https://doi.org/10.24191/esteem.v21iSeptember.7132.g5031

*Determination of the overall rate determining step*

Assuming that adsorption (Reaction 3) and desorption (Reaction 5) are rapid and reach equilibrium relative to the surface reaction (Reaction 4), the overall rate is governed by the slower surface reaction step. This simplification aligns with the Langmuir–Hinshelwood kinetic framework and allows the overall reaction rate to be expressed as:

$$-r_{H2O2} = k_{sr} C_{FA•S} C_{H2O2}$$

This expression forms the basis for deriving the overall rate law under the assumption that surface reaction kinetics are the controlling mechanism. The following derivation outlines the expressions for each step and leads to the final rate law:

Adsorption step (Reaction 3):

$$FA + S \underset{k_{-ad}}{\overset{k_{ad}}{\leftrightarrow}} FA•S$$

$$r_{ad,forward} = k_{ad}C_{FA}C_v$$

$$r_{ad,reverse} = k_{-ad}C_{FA•S}$$

$$r_{ad} = k_{ad}C_{FA}C_v - k_{-ad}C_{FA•S}$$

$$*K_{ad} = k_{ad}/k_{-ad} = K_{FA}$$

$$r_{ad} = k_{ad}[C_{FA}C_v - (C_{FA•S}/ K_{ad})]$$

Surface reaction step (Reaction 4):

$$FA•S + H_2O_2 \rightarrow PFA•S + H_2O$$

$$r_{sr} = k_{sr}C_{FA•S}C_{H2O2}$$

Desorption Step (Reaction 5):

$$PFA•S \underset{k_{-des}}{\overset{k_{des}}{\leftrightarrow}} PFA + S$$

$$r_{des,forward} = k_{des}C_{PFA•S}$$

$$r_{des,reverse} = k_{-des}C_{PFA}C_v$$

$$r_{des} = k_{des}C_{PFA•S} - k_{-des}C_{PFA}C_v$$

$$*K_{des} = k_{des}/k_{-des}$$

$$r_{des} = k_{des}[C_{PFA•S} - (C_{PFA}C_v/ K_{des})]$$

$$*K_{PFA} = 1/K_{des}$$

$$r_{des} = k_{des}[C_{PFA•S} - C_{PFA}C_vK_{PFA}]$$

Since surface reaction (Reaction 4) is the rate determining step, the kinetic study for the overall reaction is:

$$r_{sr} = -r_{H2O2} = k_{sr}C_{FA•S}C_{H2O2}$$

The overall rate is taken based on the rate of hydrogen peroxide due to its acting as the limiting reactant in this epoxidation. Reaction 4 is assumed to be an elementary, thus its rate constant ($k_{sr}$) becomes

https://doi.org/10.24191/esteem.v21iSeptember.7132.g5031

second-order in the reaction. By assuming pseudo-steady state approximation (PSSA) for adsorption (Reaction 3) and desorption (Reaction 5) reactions,

$*0 \approx r_{ad}/k_{ad}$ and $*0 \approx r_{des}/k_{des}$

$C_{FA\bullet s} = K_{FA}\, C_{FA} C_v$

$C_{PFA\bullet s} = K_{PFA}\, C_{PFA} C_v$

Applying the site balances:

$C_t = C_v + C_{FA\bullet S} + C_{PFA\bullet S}$

$C_t = C_v + K_{FA}\, C_{FA} C_v + K_{PFA}\, C_{PFA} C_v$

$C_t = C_v\,[1 + K_{FA}\, C_{FA} + K_{PFA}\, C_{PFA}]$

$C_v = C_t / [1 + K_{FA}\, C_{FA} + K_{PFA}\, C_{PFA}]$

Therefore, the overall rate law becomes:

$-r_{H2O2} = k_{sr}\, C_{FA\bullet S}\, C_{H2O2}$

$-r_{H2O2} = k_{sr}\, (K_{FA}\, C_{FA} C_v)\, C_{H2O2}$

$-r_{H2O2} = k_{sr}\, (K_{FA}\, C_{FA})\, C_{H2O2}\, C_t / (1 + K_{FA}\, C_{FA} + K_{PFA}\, C_{PFA})$

This expression reflects a second-order surface reaction rate limited by hydrogen peroxide concentration, with site coverage effects from formic and performic acid captured in the denominator.

$*k_{sr} = k_{sr} K_{FA} C_t$

The kinetic behaviour of the *in situ* epoxidation of PKO using zeolite ZSM-5 was modelled using the following rate expression derived from the Langmuir–Hinshelwood mechanism:

$-r_{H2O2} = k_{sr} C_{FA} C_{H2O2} / (1 + K_{FA}\, C_{FA} + K_{PFA}\, C_{PFA})$

The model was validated by comparing predicted and experimental RCO% values across three temperatures (45 °C, 55 °C, and 65 °C), as shown in Fig. 7, Fig. 8. and Fig. 9., respectively. Regression analysis using Polymath yielded an $R^2$ of ~0.96, demonstrating excellent agreement and confirming the reliability of the kinetic model under varied thermal conditions.

The surface reaction rate constant, $k_{sr}$, was determined using non-linear regression techniques implemented in Polymath. The calculated values of $k_{sr}$ at 318 K, 328 K, and 338 K are shown in Table 3. The constants were found to be 3.019923, 14.67545, and 81.58234 $L^2/(mol \cdot s \cdot g$ catalyst), respectively, reflecting the expected temperature dependence of surface reaction rates.

Table 3. Calculated value for surface reaction constant ($k_{sr}$)

| Temperature (K) | $k_{sr}$, ($L^2$/mol.s. g catalyst) |
|---|---|
| 318 | 3.019923 |
| 328 | 14.67545 |
| 338 | 81.58234 |

https://doi.org/10.24191/esteem.v21iSeptember.7132.g5031

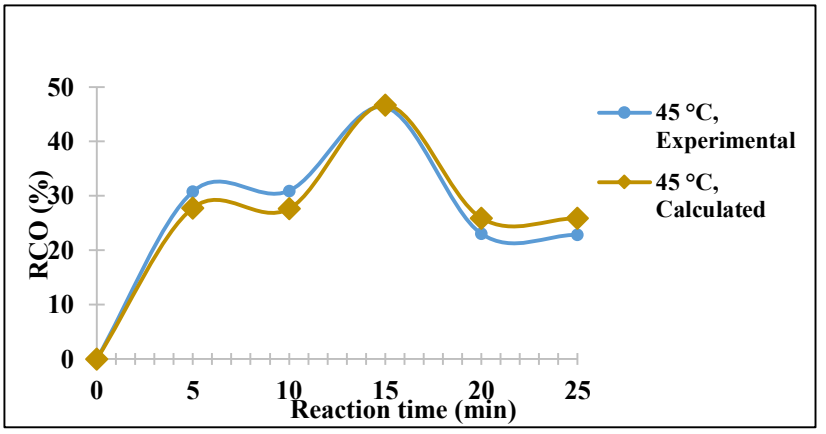


Fig. 7. Comparison between experimental and calculated RCO% for 45 °C

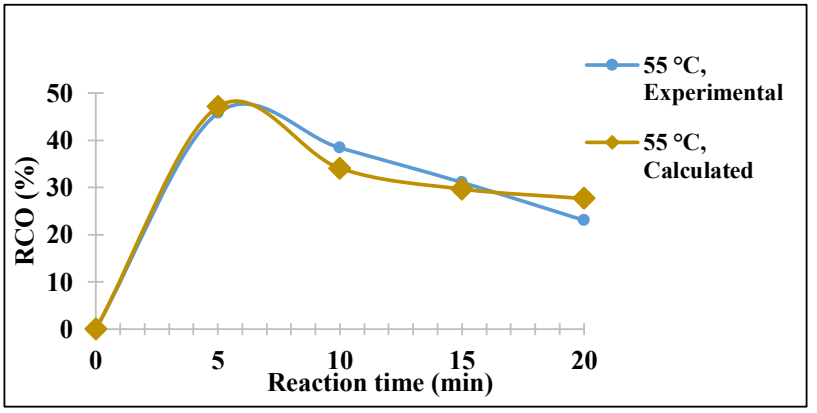


Fig. 8. Comparison between experimental and calculated RCO% for 55 °C

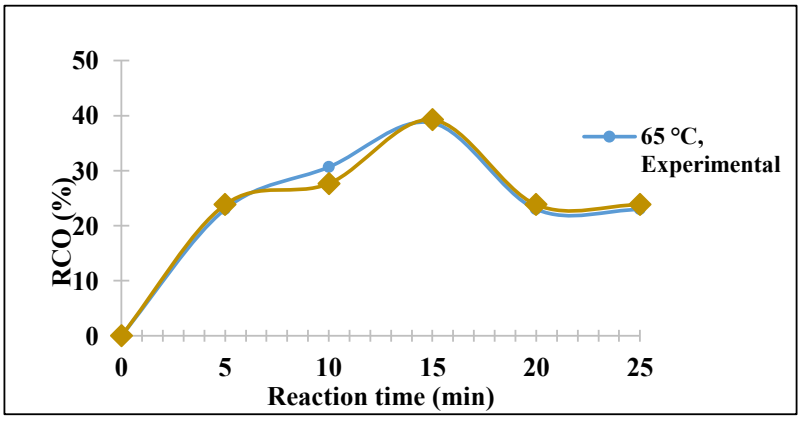


Fig. 9. Comparison between experimental and calculated RCO% for 65 °C

https://doi.org/10.24191/esteem.v21iSeptember.7132.g5031

*Determination of activation energy, $E_a$*

The activation energy for the reaction was determined through analysis of the Arrhenius plot, as illustrated in Fig. 10. Using the linearised form of the Arrhenius equation, the activation energy ($E_a$) can be derived from the slope of the plot:

$$\ln (k) = (-E_a/R) (1/T) + \ln (A)$$

Therefore,

$$\text{Slope} = (-E_a/R) = 17709$$

Substituting the universal gas constant, R = 8.314 J/mol·K into the equation:

$$E_a = - (-17709) \times 8.314 = 147232.63 \text{ J/mol} = 147.23 \text{ kJ/mol}$$

The reaction kinetics show a strong dependence on temperature. The measured activation energy of approximately 147 kJ/mol is relatively high, suggesting that the rate-limiting step involves surface-mediated processes, such as chemisorption and epoxide formation, rather than simple diffusion. This observation supports the application of a heterogeneous Langmuir–Hinshelwood (L–H) model, in which both the *in situ* generated peracid (i.e., performic acid) and the unsaturated oil molecules adsorb onto active acid sites.

As expected, increasing the reaction temperature enhances both the desired epoxide formation and unwanted side reactions. In particular, excessive heating beyond 65 °C promotes nucleophilic ring-opening of the oxirane, thereby lowering the oxirane yield. Studies report that oxirane selectivity declines sharply at higher temperatures due to epoxide cleavage. For instance, Freites-Aguillera *et al.* [32] observed a marked decrease in oxirane yield during tall-oil epoxidation at elevated temperatures, as ring-opening reactions became predominant. This behavior underscores the need for moderate operating temperatures and supports using L–H kinetic models for mechanistic interpretation. The relatively high activation energy (~147 kJ/mol) falls within the typical range for surface reaction–controlled processes (>20 kJ/mol), reinforcing the conclusion that the system is kinetically controlled rather than limited by external mass transfer [33].

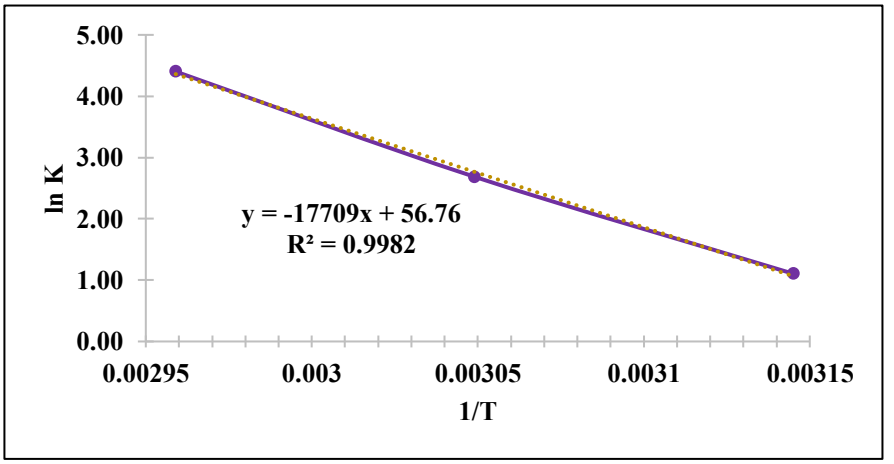


Fig. 10. The Arrhenius plot

https://doi.org/10.24191/esteem.v21iSeptember.7132.g5031

## 4. CONCLUSION

The *in situ* epoxidation of PKO was successfully carried out using zeolite ZSM-5 as a heterogeneous solid acid catalyst. Although $TiO_2$ demonstrated superior performance in maintaining epoxide ring stability, zeolite ZSM-5 achieved significantly higher oxirane conversion (RCO%) under identical reaction conditions. Based on the results, the optimal temperature for achieving efficient *in situ* epoxidation was determined to be 55 °C, using zeolite ZSM-5 as the catalyst. From the kinetic evaluation, the reaction followed a Langmuir–Hinshelwood (L–H) mechanism, with parameter estimation performed through non-linear regression using the Levenberg–Marquardt method. The model showed strong agreement between predicted and experimental data across various temperatures, validating the proposed mechanism. The calculated activation energy of 147.23 kJ/mol is consistent with surface reaction-controlled processes, confirming that the overall rate is governed by chemical kinetics rather than mass transfer limitations. These findings highlight the catalytic efficiency of zeolite ZSM-5 for PKO epoxidation and support its application in green oxidation technologies. The integrated mechanistic–kinetic approach adopted here provides a useful framework for the rational design and optimisation of heterogeneous catalytic systems for epoxidation of bio-based feedstocks.

## 5. ACKNOWLEDGEMENTS/FUNDING

The authors would like to thank the Faculty of Chemical Engineering, Universiti Teknologi MARA Shah Alam, Selangor, for the use of services and facilities in conducting the research leading to this manuscript.

## 6. CONFLICT OF INTEREST STATEMENT

The authors agree that this research was conducted in the absence of any self-benefits, commercial or financial conflicts, and declare the absence of conflicting interests with the funders.

## 7. AUTHORS' CONTRIBUTIONS

**Nur Amira Dewi Zulkifli Selvakummar**: Conceptualisation, methodology, formal analysis, investigation, and writing-original draft; **Siti Khatijah Jamaludin**: Conceptualisation, methodology, supervision, writing-review, and editing; **Siti Aminah Md Ali**: Editing and validation.

## 8. REFERENCES

[1] E. T. Phuah *et al.*, "Nonconventional Technologies in Lipid Modifications," *Annu. Rev. Food Sci. Technol.*, vol. 15, no. 1, pp. 409–430, 2024. Available: https://doi.org/10.1146/annurev-food-072023-034440

[2] A. Zbikowska, S. Onacik-Gür, M. Kowalska, K. Zbikowska, and M. Feszterová, "Trends in Fat Modifications Enabling Alternative Partially Hydrogenated Fat Products Proposed for Advanced Application," *Gels*, vol. 9, no. 6, 2023. Available: https://doi.org/10.3390/gels9060453

[3] A. M. Alhaji, E. S. Almeida, C. R. Carneiro, C. A. S. da Silva, S. Monteiro, and J. S. dos R. Coimbra, "Palm Oil (Elaeis guineensis): A Journey through Sustainability, Processing, and Utilization," *Foods*, vol. 13, no. 17, p. 2814, 2024. Available: https://doi.org/10.3390/foods13172814

[4] M. H. Wondi, N. I. N. Haris, R. Shamsudin, R. Yunus, M. Mohd Ali, and A. H. Iswardi, "Development and testing of an oil palm (Elaeis guineensis Jacq.) fruit digester process for kernel free in crude palm oil production," *Ind. Crops Prod.*, vol. 208, no. July 2023, p. 117755, 2024.

https://doi.org/10.24191/esteem.v21iSeptember.7132.g5031

Available: https://doi.org/10.1016/j.indcrop.2023.117755

[5] D. Ansorena, R. Ramírez, A. Lopez de Cerain, A. Azqueta, and I. Astiasaran, "Oxidative Stability and Genotoxic Activity of Vegetable Oils Subjected to Accelerated Oxidation and Cooking Conditions," *Foods*, vol. 12, no. 11, pp. 1–16, 2023. Available: https://doi.org/10.3390/foods12112186

[6] S. García-Maza, S. Rojas-Flores, and Á. D. González-Delgado, "Technical Insights into Crude Palm Oil (CPO) Production Through Water–Energy–Product (WEP) Analysis," *Sustain.*, vol. 17, no. 10, pp. 1–12, 2025. Available: https://doi.org/10.3390/su17104485

[7] F. Rico *et al.*, "Meta-Analysis and Analytical Methods in Cosmetics Formulation: A Review," *Cosmetics*, vol. 11, no. 1, 2024. Available: https://doi.org/10.3390/cosmetics11010001

[8] Y. Zeng *et al.*, "A Review of Chemical Modification of Vegetable Oils and Their Applications," *Lubricants*, vol. 12, no. 5, 2024. Available: https://doi.org/10.3390/lubricants12050180

[9] O'Brien, R.D., *Fats and Oils: Formulating and Processing for Applications*, Third Edition (3rd ed.). CRC Press, 2008. Available: https://doi.org/10.1201/9781420061673R

[10] N. H. Rahim, M. J. Jalil, N. M. Mubarak, I. S. Azmi, and G. Anbuchezhiyan, "Catalytic epoxidation of unsaturated fatty acids in palm stearin via in situ peracetic acids mechanism," *Sci. Rep.*, vol. 15, no. 1, pp. 1–12, 2025. Available: https://doi.org/10.1038/s41598-025-89399-x

[11] M. L. Mohammed and B. Saha, "Recent Advances in Greener and Energy Efficient Alkene Epoxidation Processes," *Energies*, vol. 15, no. 8, 2022. Available: https://doi.org/10.3390/en15082858

[12] Y. Shen, P. Jiang, P. T. Wai, Q. Gu, and W. Zhang, "Recent progress in application of molybdenum-based catalysts for epoxidation of alkenes," *Catalysts*, vol. 9, no. 1, 2019. Available: https://doi.org/10.3390/catal9010031

[13] C. Cheng, Z. Wei, X. Ming, J. Hu, and R. Kong, "Study on Reaction Mechanism and Process Safety for Epoxidation," *ACS Omega*, vol. 8, no. 49, pp. 47254–47261, 2023. Available: https://doi.org/10.1021/acsomega.3c07461

[14] D. N. A. Raofuddin *et al.*, "Epoxidation of Unsaturated Oleic Acids via in Situ Catalytic Performic Acid," *Iran. J. Chem. Chem. Eng.*, vol. 42, no. 5, pp. 1491–1498, 2023. Available: https://doi.org/10.30492/ijcce.2022.557155.5425

[15] N. Mohd Zin, S. K. Jamaludin, H. Hassan, Z. Wan, A. K. Nur Fadzeelah, and S. Mohd Sukri, "Effect of Oxygen Carrier and Reaction Temperature in Enhancing the Epoxy Ring Stability in the Epoxidation of Palm Kernel Oil," *IOP Conf. Ser. Mater. Sci. Eng.*, vol. 864, no. 1, 2020. Available: https://doi.org/10.1088/1757-899X/864/1/012024

[16] F. Marriam, A. Irshad, I. Umer, M. A. Asghar, and M. Atif, "Vegetable oils as bio-based precursors for epoxies," *Sustain. Chem. Pharm.*, vol. 31, no. December 2022, p. 100935, 2023. Available: https://doi.org/ 10.1016/j.scp.2022.100935

[17] T. I. Cooney, F. Cardona, and T. Tran-Cong, "Kinetics of in Situ Epoxidation of Hemp Oil Under Heterogenous Reaction Conditions : an Overview With Preliminary Results," *Energy, Environ. Sustain.*, pp. 106–111, 2011.

[18] Z. Yan, Z. Ma, J. Deng, and G. Luo, "Mechanism and kinetics of epoxide ring-opening with carboxylic acids catalyzed by the corresponding carboxylates," *Chem. Eng. Sci.*, vol. 242, p. 116746, 2021. Available: https://doi.org/10.1016/j.ces.2021.116746

[19] V. V. Goud, A. V. Patwardhan, S. Dinda, and N. C. Pradhan, "Kinetics of epoxidation of jatropha oil with peroxyacetic and peroxyformic acid catalysed by acidic ion exchange resin," *Chem. Eng. Sci.*, vol. 62, no. 15, pp. 4065–4076, 2007. Available: https://doi.org/10.1016/j.ces.2007.04.038

[20] G. Zhao *et al.*, "Research Progress in Epoxidation of Light Small-Molecule Olefins," *Molecules*,

https://doi.org/10.24191/esteem.v21iSeptember.7132.g5031

vol. 30, no. 6, pp. 1–44, 2025. Available: https://doi.org/10.3390/molecules30061340

[21] J. Ferraz-Caetano, F. Teixeira, and M. N. D. S. Cordeiro, "Systematic Development of Vanadium Catalysts for Sustainable Epoxidation of Small Alkenes and Allylic Alcohols," *Int. J. Mol. Sci.*, vol. 24, no. 15, 2023. Available: https://doi.org/10.3390/ijms241512299

[22] S. H. Chung, G. H. Park, N. Schukkink, H. Lee, and N. R. Shiju, "Structure-sensitive epoxidation of dicyclopentadiene over TiO2 catalysts," *Chem. Commun.*, vol. 59, no. 6, pp. 756–759, 2022. Available: https://doi.org/10.1039/d2cc05305e

[23] S. K. Jamaludin, K. H. Ku Hamid, H. Abu Hassan, A. Md Som, Z. Maurad, and A. Azizi, "Application of Taguchi Optimization Method in Improving the Selectivity of Dihydroxystearic Acid," *Adv. Mater. Res.*, vol. 1113, pp. 703–709, 2015. Available: https://doi.org/10.4028/www.scientific.net/amr.1113.703

[24] J.B., "The determination of epoxide groups," *J. Mol. Struct.*, vol. 9, no. 4, p. 491, 1971. Available: https://doi.org/ 10.1016/0022-2860(71)87047-3

[25] N. Mohamed, M. J. Jalii, S. K. Jamaludin, and A. R. M. Daud, "Formation of Dihydroxystearic Acid from Hydrolysis of Palm Kernel Oil Based Epoxidized Oleic Acid Mohd Jumain Jalil," *J. Appl. Sci. Agric.*, vol. 9, no. 11, pp. 86–92, 2014, [Online]. Available: https://www.researchgate.net/publication/275894216

[26] L. E. Manangon-Perugachi *et al.*, "Mesoporous methyl-functionalized titanosilicate produced by aerosol process for the catalytic epoxidation of olefins," *Catalysts*, vol. 11, no. 2, pp. 1–19, 2021. Available: https://doi.org/10.3390/catal11020196

[27] N. Grifasi, F. A. Deorsola, D. Fino, and M. Piumetti, "Mesoporous TiO2 and Fe-containing TiO2 prepared by solution combustion synthesis as catalysts for the photodegradation of paracetamol," *Environ. Sci. Pollut. Res.*, vol. 31, no. 25, pp. 36861–36881, 2024. Available: https://doi.org/10.1007/s11356-024-33575-5

[28] S. Ding *et al.*, "Spatial segregation of catalytic sites within Pd doped H-ZSM-5 for fatty acid hydrodeoxygenation to alkanes," *Nat. Commun.* , vol. 15, no. 1, pp. 1–12, 2024. Available: https://doi.org/ 10.1038/s41467-024-51925-2

[29] M. A. Saritala, M. Muzammil, M. R. Quddus, S. A. Razzak, and M. M. Hossain, "A Review on Production of Ethylene Oxide from Epoxidation of Ethylene : Catalysis , Mechanism and Kinetics," pp. 1–24, 2025.

[30] P. Mäki-arvela, E. A. Alarcón, and P. Serrano, "for the valorization of monoterpene epoxides †," vol. 27, no. ii, pp. 10512–10528, 2024. Available: https://doi.org/10.1039/d4gc04003a

[31] F. Y. Fredrick, A. M. Abdullahi, M. N. Ibrahim, M. B. Chiroma, and A. A. Girbo, "Extraction, Characterization and Epoxidation of Castor Seed Oil," *Fudma J. Sci.*, vol. 7, no. 2, pp. 284–288, 2023. Available: https://doi.org/10.33003/fjs-2023-0702-1987

[32] A. Freites Aguilera, *Epoxidation of vegetable oils – Process intensification for biomass conversion*. 2019.

[33] K. A. Ahmad, S. F. Elahi, H. Znad, and E. Ahmad, "Kinetic and mechanistic investigation of Butyl Levulinate synthesis on ZSM-5 supported phosphomolybdic acid," *Sci. Rep.*, vol. 15, no. 1, pp. 1–19, 2025. Available: https://doi.org/10.1038/s41598-025-89953-7



https://doi.org/10.24191/esteem.v21iSeptember.7132.g5031